Ceramics International 46 (2020) 10667–10677

Contents lists available at ScienceDirect

Ceramics International

journal homepage: www.elsevier.com/locate/ceramint

Enhanced photocatalytic activity under visible light by the synergistic effects of plasmonics and Ti^{3+}-doping at the Ag/TiO_{2-x} heterojunction

Lianying Lu[a], Guohong Wang[a,*], Ziwei Xiong[a], Zifei Hu[a], Yuwei Liao[a], Juan Wang[a], Jun Li[b,**]

[a] Hubei Key Laboratory of Pollutant Analysis and Reuse Technology, College of Chemistry and Chemical Engineering, Institute for Advanced Materials, Hubei Normal University, Huangshi, 435002, PR China

[b] Department of Chemistry, Kansas State University, Manhattan, KS, 66506, USA

ARTICLE INFO

Keywords:
Macroporous/mesoporous TiO_2 microchannel
Ti^{3+}-doped TiO_2
Ag/TiO_{2-x} heterojunction
Surface plasmon resonance
Photocatalysis

ABSTRACT

A heterojunction of plasmonic Ag particles on Ti^{3+}-doped macro-/meso-porous TiO_2 framework consisting of parallel microchannels, denoted as Ag/TiO_{2-x}, has been fabricated by a simple microwave-assisted process employing vitamin C as the reducing agent for forming TiO_{2-x} framework followed by photochemical deposition of Ag particles. Charge transport and recombination processes were detected through transient photocurrent responses. The visible-light photocatalytic hydrogen production rate and the apparent reaction rate constant of RhB photodegradation with 3%-Ag/TiO_{2-x} catalyst are about 5.3 and 14.0 fold higher than those with the pristine macro-/meso-porous TiO_2 framework, respectively. A mechanism based on the synergistic effects of Ag plasmonics and Ti^{3+}-doping at the Ag/TiO_{2-x} heterojunction is proposed, which consistently explains the high photocatalytic performance in hydrogen evolution and the improved photocatalytic decomposition of RhB under visible light. This study demonstrates the effective route to synthesize new heterojunction photocatalytic materials with multifunctional properties using low-cost and rapid microwave processes.

1. Introduction

The crisis of fossil energy and distruction of ecologic environment are the two severe issues that we are facing today [1–3]. Currently, one of the most prospective paths for alleviating these problems is photocatalysis [4–7], due to its great potential for splitting water into hydrogen fuel, CO_2 photoreduction into renewable hydrocarbon fuel [8–13], photodegradation of organic pollutants [14–20], generation of electricity with dye-sensitized solar cells [21], and the removal of toxic gases [22,23]. The development of suitable photocatalysts is key to these research that can induce chemical reactions not feasible in dark conditions by effectively harvesting photons [24]. TiO_2 is believed to be one of the forerunner semiconductor photocatalysts owing to its unique physical and chemical properties, such as excellent chemical stability, low cost and environmental compatibility [25]. However, as a photocatalyst, application of TiO_2 is restricted by its rapid recombination of photoexcited charge carriers and wide band gap. To overcome these problems, strategies were employed by doping with metal, nonmetal and lower-valence state Ti^{3+} (or oxygen vacancies) [26–34], surface sensitization [35], coupling with narrower band gap semiconductors [36–40], etc. In addition, TiO_2 has been incorporated in many hybrid materials to form heterojunction photocatalysts, thereby giving lower electron-hole recombination rate and broader-band photon absorption [41].

Among the various methods, integrating noble metal nanoparticles, such as Au and Ag with TiO_2 is a promising strategy. The photocatalytic performance can be significantly enhanced because of the localized surface plasmon resonance (SPR) induces strong absorption of visible light and improves photogenerated charge separation at the metal-semiconductor interface [42–44]. Furthermore, the Ag and Au nanoparticles are chemically stable in many photocatalytic reactions and their SPR performance can be controlled by tuning their size, shape and assembly on the TiO_2 surface, giving larger freedom to optimize the photocatalyst.

Ti^{3+} self-doping has been proven to be another effective approach. Usually, Ti^{3+}-doped TiO_2 presents dark blue or black color due to the introduction of oxygen vacancy (O_V) states in the band gap of TiO_2, and generates a strong absorption of visible light. Also, the formation of structural defects is able to capture electrons, hinder the recombination of the e^--h^+ pairs, improve the electrical conductivity, facilitate electron transfer and hydrogen desorption, and thereby remarkably enhance photocatalytic activity and photoelectrochemical (PEC) property

* Corresponding author.
** Corresponding author.
E-mail addresses: wanggh2003@163.com (G. Wang), junli@ksu.edu (J. Li).

https://doi.org/10.1016/j.ceramint.2020.01.073
Received 28 October 2019; Received in revised form 5 January 2020; Accepted 9 January 2020
Available online 10 January 2020

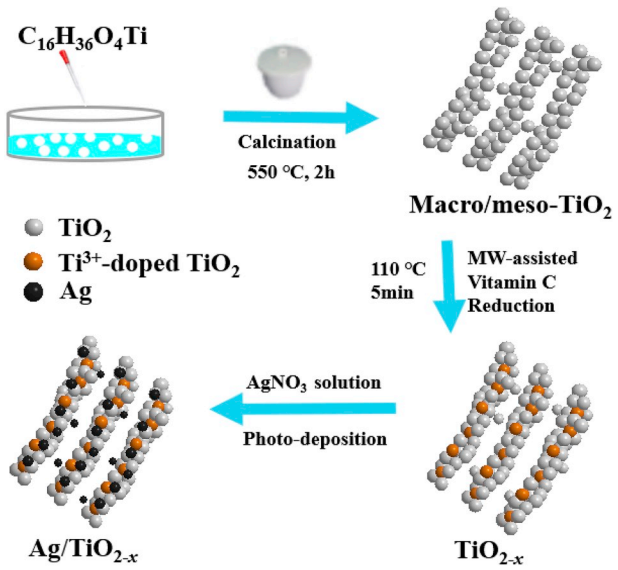

Fig. 1. Schematic diagram of the procedure to prepare Ag/TiO_{2-x} photocatalysts.

of TiO_2 [45–47]. Therefore, many research have been devoted to preparing Ti^{3+}-doped black TiO_2 with various methods, for example hydrogenation, chemical reduction/oxidation, anodization, electrochemical reduction, and Al vapor reduction in high-pressure and high-temperature [48–52]. However, these methods frequently demand expensive equipment and harsh preparation conditions, raising safety and sustainability concerns. Therefore, it is fully necessary to explore a method for synthesizing Ti^{3+}-doped TiO_2 at milder conditions.

Herein, we develop a simple microwave-assisted process to synthesize Ti^{3+}-doped TiO_2 (i.e., TiO_{2-x}) using vitamin C as the reducing agent. It is then followed by a photo-reduction process to deposit Ag nanoparticles and form Ag/TiO_{2-x} composites (see Fig. 1). The Ag/TiO_{2-x} composites with varied Ag contents have been employed as photocatalysts for photocatalytic production of H_2 and photocatalytic degradation for RhB using visible light. The Ag/TiO_{2-x} composites show drastically improved photocatalytic activities as compared to pristine TiO_2, Ti^{3+}-doped TiO_2 (denoted as TiO_{2-x}) and Ag/TiO_2 hybrids. The results reveal a strong synergistic enhancement by the combination of the plasmonic effect of Ag nanoparticles and heavy Ti^{3+}-doping, which is particularly effective for improving photocatalysis using broad-band visible light. By our knowledge, this has not been reported in the literatures. This phenomenon provides new insights into tuning TiO_2 properties for higher photocatalytic activities by safe, low-cost and reliable synthetic routes.

2. Experimental section

2.1. Materials

Tetrabutyltitanate (TBOT, $C_{16}H_{36}O_4Ti$) and triethanolamine ($C_6H_{15}NO_3$) were purchased from Sinopharm Chemical Reagent Co., Ltd. Vitamin C and silver nitrate ($AgNO_3$) were purchased from Aladdin. All chemicals are analytical grade. Double-distilled water was employed in this research.

2.2. Photocatalysts preparation

A facile microwave-assisted method was employed to prepare the Ag/TiO_{2-x} composites. The synthesis of the pristine macro-/meso-porous TiO_2 framework was described in our previous studies [38,40]. The 0.3 g of pristine powdered TiO_2 was added into 20 mL of aqueous solution with 3.3 g vitamin C. The above suspension was treated by ultrasonication for 15 min and then transferred into a 30 mL glass vial to be used in an automatically controlled microwave reactor (Discover SP 909155, Matthews. NC, USA). The solution was heated to 110 °C by microwave radiation with an output power of 30 W under atmospheric pressure for 5 min with gentle magnetic stirring. Further washing by water and desiccating at 60 °C led to the Ti^{3+}-doped TiO_2, denoted as TiO_{2-x}. At last, 0.4 g of TiO_{2-x} powder was mixed with 0.0064, 0.0192 and 0.0320 g $AgNO_3$ in 50 mL water under vigorous stirring for 30 min, respectively. After that, the mixture was irradiated with a 350 W Xenon lamp for 30 min. Then the above mixture was filtered, washed thoroughly with distilled water and dried at 80 °C for 10 h. Samples were denoted as y%-Ag/TiO_{2-x}, where y represents the mass ratio of Ag to TiO_2, as 1%, 3%, and 5%, respectively. The Ag/TiO_2 control sample was prepared following the identical procedures described previously, by using the pristine macro-/meso-porous TiO_2.

2.3. Materials characterization

The crystallographic structures of the as-obtained photocatalysts were confirmed with powder X-ray diffraction (Bruker AXS, German). X-ray photoelectron spectroscopy (XPS, VG Escalab 220i-XL, UK) was tested under a monochromatic Al Kα source. To observe the morphology, SEM, HRTEM and STEM images were obtained by a S–3400 N (Hitachi, Japan) scanning electron microscope and a FEI talos 200X (FEI, USA) transmission electron microscope operating at an acceleration voltage of 200 kV, respectively. The EPR (electron paramagnetic resonance) spectra were performed with a MEX-nano spectrometer (Bruker, German). The pore size distribution and BET surface area of the prepared samples were analyzed by ASAP 2020HD 88 instrument (Micromeritics, USA). UV–vis absorption spectra of the samples were obtained with a UV–vis 2550 spectrophotometer (Shimadzu, Japan) using $BaSO_4$ as a reference.

2.4. Photocatalytic activity test

The photocatalytic performance of the as-obtained catalysts was evaluated with average rates for hydrogen production and Rhodamine B decomposition. In the photocatalytic reaction, a 350 W Xenon arc lamp with a 420 nm cut-off filter were used. Usually, 40 mg of the as-prepared sample was placed in 30 mL RhB solution, the evolution of concentration of RhB was recorded by UV–vis spectrophotometer at the wavelength of 552 nm.

For the photocatalytic hydrogen production experiment, first, 50 mg of the photocatalyst was added into 100 mL triethanolamine ($C_6H_{15}NO_3$, 20 vol%) sacrificial agent aqueous solution. Subsequently, the suspension was sonicated for 20 min [53]. The photocatalyst suspension was deaerated by nitrogen gas for 30 min. Then, the photocatalytic reaction was triggered by visible light irradiation under magnetic stirring at room temperature. The gaseous products were gathered for 0.5 h interval with a gas-tight syringe [54] and the photocatalytic H_2 evolution was evaluated through a gas chromatograph (SP7820, Limited, China).

2.5. Electrochemical performances test

The photocurrent response was detected on an electrochemical station (CHI660E/700E, Shanghai Chenhua, China). First, the as-prepared samples were smeared on a FTO glass by spin coating as the working electrode, and an Ag/AgCl electrode and a Pt foil were employed as the reference electrode and the counter electrode, respectively. Then, the three electrodes were inserted in the 0.5 M Na_2SO_4 electrolyte solution. At last, the solution was purged for 0.5 h with N_2. The photocurrents and EIS measurements were measured under visible light illumination using a LED lamp (420 nm, 3 W).

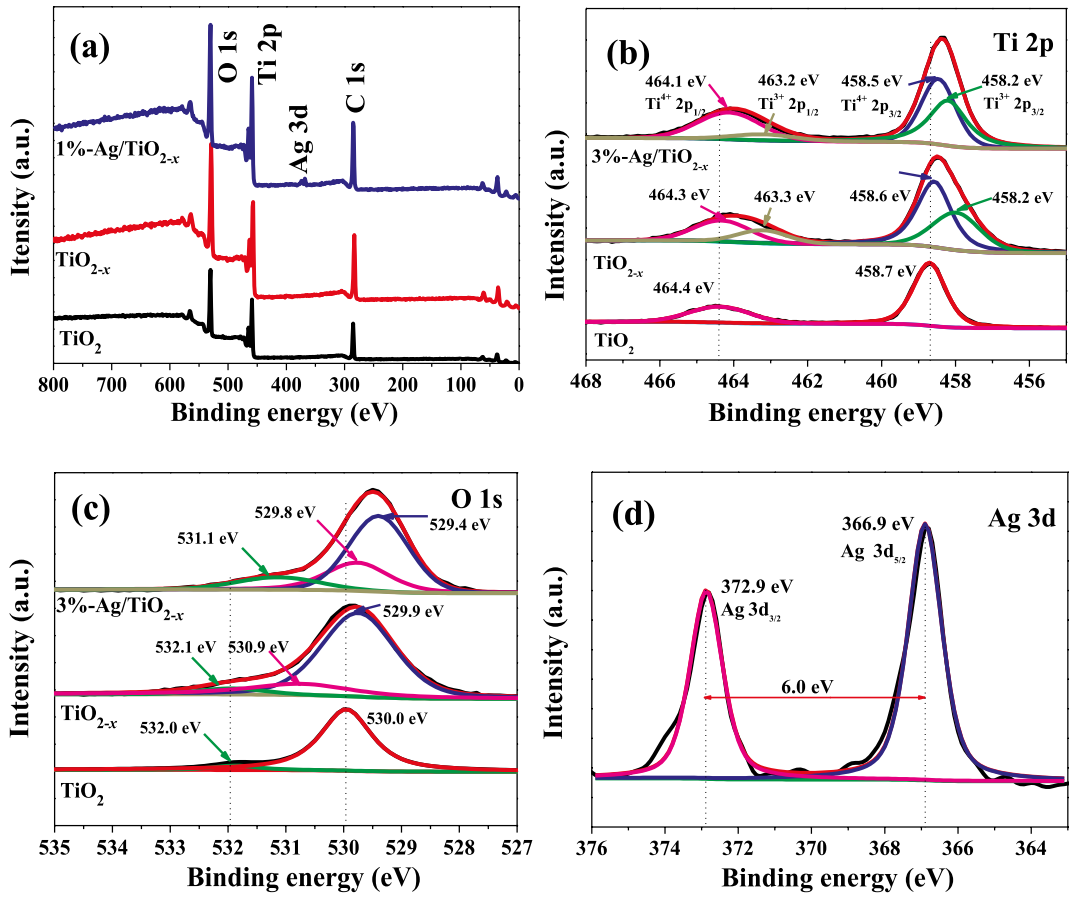

Fig. 2. (a) XPS survey spectra, (b) Ti 2p and (c) O 1s high-resolution XPS spectra of pure TiO_2, TiO_{2-x} and 3%-Ag/TiO_{2-x}, and (d) Ag 3d XPS spectrum of 3%-Ag/TiO_{2-x}.

3. Results and discussion

3.1. Composition, morphology and structure of catalysts

To determine the chemical composition of the catalysts, XPS (X-ray photoelectron spectroscopy) was employed. Fig. 2a displays the measured spectra of pristine TiO_2, TiO_{2-x} and 3%-Ag/TiO_{2-x} samples. The XPS spectra of the bare TiO_2 and TiO_{2-x} samples are almost identical. All XPS spectra show feature peaks belong to Ti, O and C, whereas it is clear that a small amount of element Ag is present in 3%-Ag/TiO_{2-x}. The C 1s peak is attributed to adventitious hydrocarbon contamination from the instrument [23]. In the Ti 2p region of TiO_{2-x} (Fig. 2b), the peaks appearing at 458.6 and 464.3 eV are assigned to Ti $2p_{3/2}$ and Ti $2p_{1/2}$ of the Ti^{4+}, while the peaks located at 458.2 and 463.3 eV belong to $2p_{3/2}$ and $2p_{1/2}$ of the Ti^{3+}, respectively [25]. The presence of the peak of Ti^{3+} confirms that a part of Ti^{4+} has been successfully reduced by vitamin C [16,27]. Simultaneously, compared with pure TiO_2, the Ti 2p peaks of TiO_{2-x} show a slight decrease in the band energy, indicating that vitamin C reduction produces more Ti^{3+} [3]. Interestingly, the Ti 2p peaks of 3%-Ag/TiO_{2-x} shift to a lower band energy by *ca.* 0.2 eV as compared to those of the TiO_{2-x} sample. This may be due to the fact that during the photo-deposition of Ag metal, some electrons migrate from Ag to Ti^{4+} and cause it to form Ti^{3+} ($Ag + e^- \rightarrow Ag^-$, $Ag^- + Ti^{4+} \rightarrow Ti^{3+} + Ag$) [21].

As revealed in Fig. 2c, the O 1s peak in the pristine TiO_2 sample can be fitted with two major peaks corresponding to the lattice oxygen (530.0 eV) and surface hydroxyl oxygen (532.0 eV), respectively. But three fitted O 1s peaks are observed in TiO_{2-x}, among which the two peaks focused at 529.9 and 532.1 eV are attributed to Ti–O and O–H, respectively [54]. Furthermore, the third peak appearing at 530.9 eV is attributed to the oxygen vacancies (O_V) near Ti^{3+}. These data clearly indicate the presence of Ti^{3+} [52]. Since the charge associated with Ti^{3+} in titanium dioxide needs to be balanced by oxygen vacancies [54], O_V generally appears in pair with Ti^{3+}. The Ti 2p and O 1s peak in the XPS spectra show the presence of Ti^{3+} and oxygen vacancies in the compound, which is beneficial in reducing the band gap and promoting separation and transfer of photo-excited e^--h^+ pairs [25]. In addition, the integrated peak area of the oxygen vacancy in 3%-Ag/TiO_{2-x} is significantly higher, indicating that more oxygen vacancies are formed in the composite [3,15], which is in consistent with the bare TiO_{2-x} sample. Fig. 2d displays the Ag 3d spectra of representative 3%-Ag/TiO_{2-x} sample. In Ag 3d region, the peaks corresponding to Ag $3d_{5/2}$ and Ag $3d_{3/2}$ are located at 366.9 eV and 372.9 eV, respectively [25]. There is a difference of 6.0 eV between binding energies of Ag $3d_{3/2}$ and $3d_{5/2}$ peaks, indicating that Ag is mainly present on the surface of TiO_2 in the Ag° state [31]. It is worth pointing out that the binding energy shows negative shifts by about −1.3 eV from 374.2 to 372.9 eV in comparison with pristine Ag. This may be due to the close contact between the Ag nanoparticles and the TiO_2, which forms a Schottky barrier with some electrons being transferred across the barrier from TiO_2 and trapped in Ag particles [23,25,31].

The microstructures of the synthetic catalysts are characterized by SEM, TEM, STEM and HR-TEM. Figs. 3a–c show the SEM images of the pristine TiO_2, TiO_{2-x} and 3%-Ag/TiO_{2-x}, respectively. In Fig. 3a, the pristine TiO_2 sample clearly displayed a unique macroporous framework with parallel microchannels whose walls possess a mesoporous structure. The morphology of Ti^{3+}-doped TiO_2 framework in Fig. 3b shows no obvious change. It can be observed that a small amount of TiO_2 particles up to *ca.* 1.0 μm are attached on the surface of the microchannels in both these two samples. The presence of such

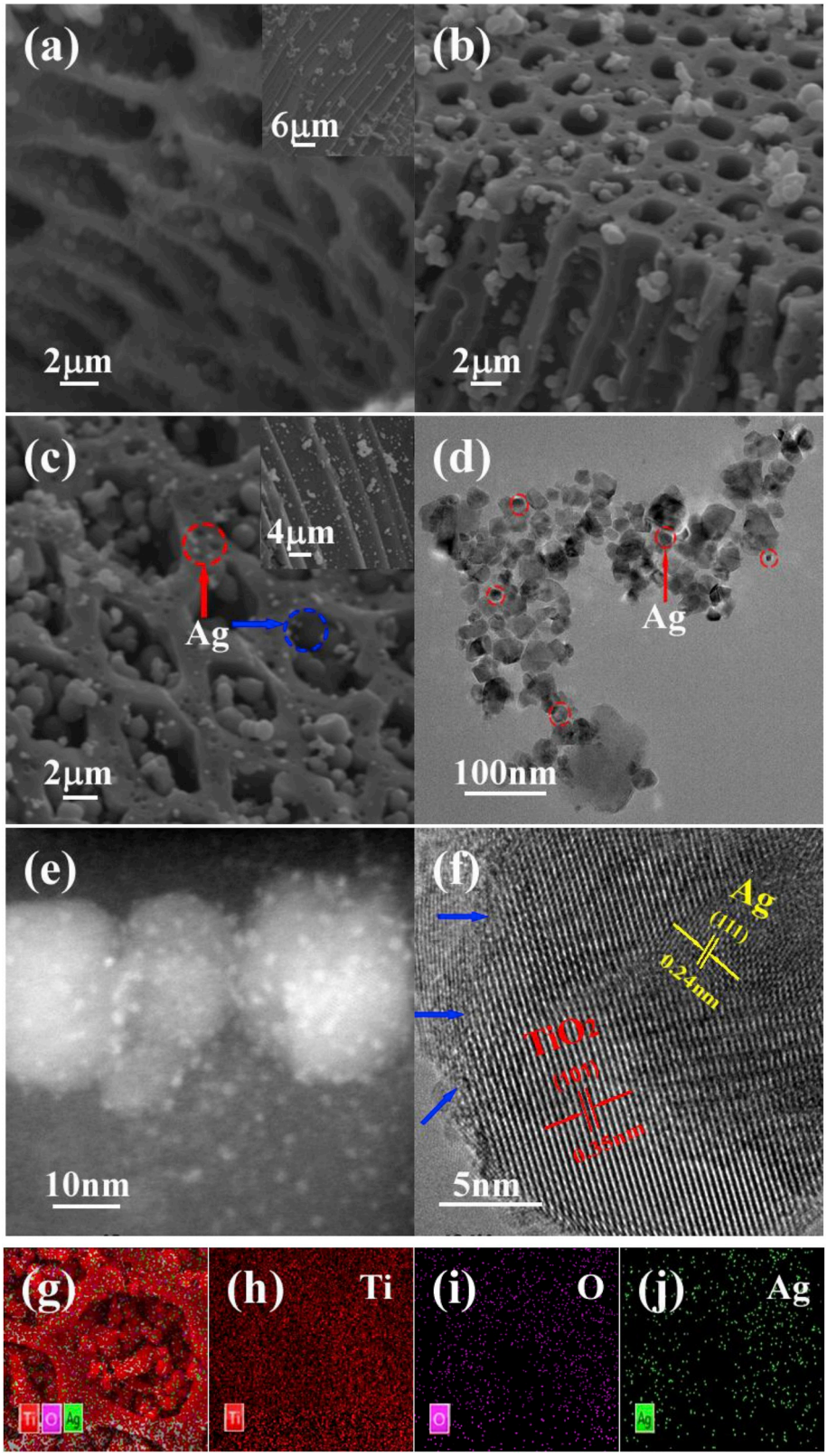

Fig. 3. SEM pictures of (a) pristine TiO_2 framework, (b) TiO_{2-x} framework, and (c) the 3%-Ag/TiO_{2-x} hybrid, (d) TEM, (e) STEM and (f) HR-TEM images of the 3%-Ag/TiO_{2-x} hybrid, (g)–(j) elemental mapping images for the 3%-Ag/TiO_{2-x} hybrid.

hierarchical macro-/meso-porous structures can maximize the surface area of the photocatalyst and accelerate the diffusion of reactants and products in the solution, resulting in enhanced photocatalytic performance [17,38]. The SEM images of the 3%-Ag/TiO_{2-x} sample in Fig. 3c show that the TiO_2 skeleton reserved the macroporous structure. However, globular Ag particles with the diameter up to 150 nm (indicated by the blue circles) were attached to internal wall of the open microchannels. Some Ag particles were also dispersed on the external

TiO_{2-x} surface (represented by the red circles) [23] and without the aggregation phenomenon [24].

The TEM image in Fig. 3d further reveals that most of the Ag nanoparticles exhibit diameters of about 10–50 nm by photoreduction method [7,17], which are randomly embedded in the TiO_2 framework, while making only close contact with each other. Thus, the Ag nanoparticles are strongly coupled with the TiO_2 surface to be conducive to photogenerated electron transfer and to effectively inhibit carrier recombination [7,23], while maintaining the SPR properties close to dispersed Ag nanoparticles.

The HAADF-STEM image (Fig. 3e) further illustrates that some even smaller silver nanoparticles of about 3–5 nm diameter attached to the larger Ag nanoparticles of 15–20 nm nanoparticles (as bright spheres in the dark field STEM) which are attached to the TiO_2 surface. Even though the size of the Ag nanoparticles varies in a large range from 3 to 150 nm, it is evident that they are well dispersed on the surface of the TiO_2 framework [33].

Fig. 3f displays the HR-TEM lattice image of 3%-Ag/TiO_{2-x}, which clearly indicates the presence of both TiO_2 and Ag particles. A slight blurring lattice (the blue arrow) in the outermost layer of the TiO_2 particles can be ascribed to the formation of the oxygen vacancy (O_V) and Ti^{3+} sites due to the reduction effect of vitamin C [15,20,26,29]. The lattice fringes with distance of 0.35 nm and 0.24 nm are resulted from the (101) plane of anatase TiO_2 and the (111) plane of cubic Ag, respectively. These results demonstrate the high crystallinity of metallic Ag phase and TiO_2 anatase phase.

The presence and distribution of the elements in the composites are further analyzed by energy dispersive X-ray spectroscopy (EDS). Figs. 3g–j present elemental mapping images of Ti, O and Ag in the 3%-Ag/TiO_{2-x} sample, confirming the Ag presence on the open microchannels and on the external TiO_{2-x} surface [27,28].

Fig. 4a shows the X-ray diffraction (XRD) patterns of all catalysts. The diffraction peaks marked with a star notation accord to anatase phase of TiO_2 (JCPDS No. 21–1272), which are very sharp, obviously meaning its highly crystalline property. Besides, the other peaks are not discovered, which represents that the as-obtained TiO_2 is highly pure anatase [17,25,52]. The XRD patterns of TiO_2 framework remain the same in the samples after Ti^{3+} doping and Ag nanoparticle deposition, illustrating that neither the self-doped Ti^{3+} and associated O_V caused by vitamin C reduction nor the Ag deposition affected the crystal structure of TiO_2 [15,30]. Although the amount of incorporated silver was small and they are highly dispersed, two weak diffraction peaks at 38.2° and 44.4° (marked with blue circles) can be observed with the of the binary systems over 3% Ag, which match exactly with the JCPDS file No. 04–0783 for Ag metal [27,28].

To verify the formation of uncoupled electrons, an EPR measurement for the as-prepared samples was conducted. As presented in Fig. 4b, the TiO_2 sample displays a small resonance signal barely above the noise level, suggesting that there is a negligible amount of Ti^{3+} in the TiO_2 framework. In contrast, a strong EPR peak at g = 2.003 was observed in the TiO_{2-x}, which can be assigned to the fact that unpaired electrons are captured by the surface oxygen vacancies [23,51]. During the microwave-assisted synthesis process, the vitamin C molecules are adsorbed on TiO_2 surface and subsequently reduce part of Ti^{4+} species into Ti^{3+} species, leading to oxygen vacancies [41]. Because the surface Ti^{3+} under room temperature is readily oxidized to Ti^{4+}or is overlapped with the strong signal of O_V, the signal of Ti^{3+} (g = 1.98) can not be observed. Therefore, we deduce that paramagnetic Ti^{3+} defects indeed exist on the sample surface. Due to the presence of the redox couple ($Ti^{4+} + e^- \rightarrow Ti^{3+}$ and $O^{2-} - e^- \rightarrow O^-$), the O_V is always

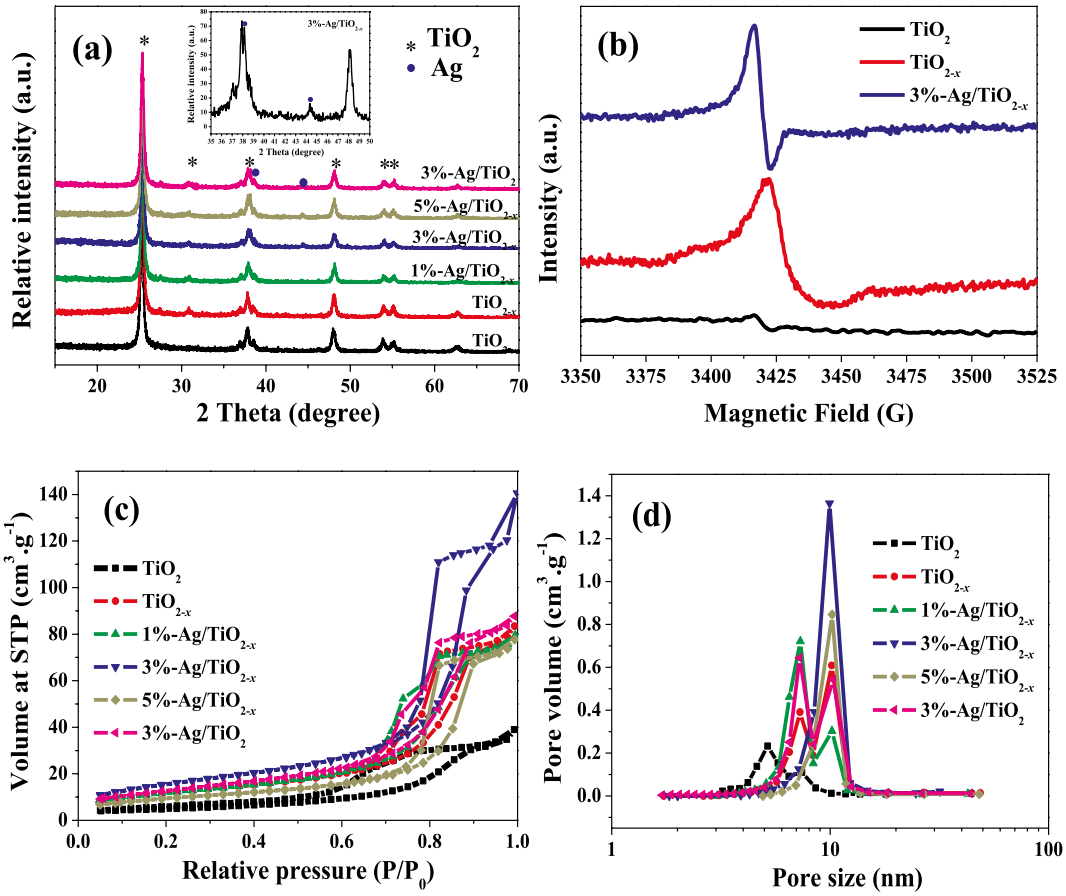

Fig. 4. (a) XRD patterns of all samples, (b) EPR spectra of TiO_2, TiO_{2-x} and 3%-Ag/TiO_{2-x} samples, (c) N_2 adsorption-desorption isotherms and (d) the corresponding pore size distribution curves of all samples.

followed by the generation of Ti^{3+} defects. Thus EPR data confirmed the existence of Ti^{3+} defects in the large quantity of the TiO_{2-x} sample [23,51]. Moreover, the 3%-Ag/TiO_{2-x} shows an obvious EPR signal, which is equivalent to g = 2.005. This indicates that a lot of more Ti^{3+} defects present on the surfaces of this sample. Accordingly, more O_V sites are induced by surface Ti^{3+}. The O_V-induced localized states are efficient for trapping charge carriers, beneficial to an enhanced photoactivity.

N_2 adsorption-desorption isotherms and the corresponding pore size distribution of the pristine TiO_2, TiO_{2-x} and various Ag/TiO_2 composite samples are plotted in Figs. 4c and d. All isotherms in Fig. 4c can be categorized to type IV with H2-type hysteresis loop according to the IUPAC definition. Moreover, they all present a high adsorption at the high relative pressure (P/P_0) range, signifying the presence of large mesopores [17,48,53]. Compared with pristine TiO_2, the N_2 adsorption-desorption isotherms of all other samples shift upward, indicating the increase of specific surface area (S_{BET}). Particularly, after the vitamin C reduction process, the S_{BET} increases from 17.1 $m^2\ g^{-1}$ for TiO_2 to 43.8 $m^2\ g^{-1}$ for TiO_{2-x}, indicating that the introduction of Ti^{3+} not only provided doping but also improved the pore structure. It is worth to note that the isotherms of Ag/TiO_{2-x} composites changed with Ag nanoparticles. The 3%-Ag/TiO_{2-x} sample presents the highest S_{BET} and well-defined pore diameter distribution around 9.9 nm (Fig. 4d). When the Ag contents were higher or lower than 3%, the specific surface area was low and the pore size distribution was not good. The surface area, pore volume and pore diameter of the as-prepared samples were listed in Table 1. Interestingly, the S_{BET} of Ag/TiO_2 is substantially higher than that of pristine TiO_2, indicating that Ag particles not only serve as the plasmonic light absorber, but also enhance the active surface area. The suitable silver loading and specific surface area are favorable to produce more reaction active sites, which can enhance the photocatalytic activities [17].

3.2. UV–vis analysis

Fig. 5a shows the UV–vis diffuse reflectance spectra (DRS) of the samples. The photos in the insets show the color of each sample. Obviously, after reduction using vitamin C, the color of the as-obtained TiO_{2-x} changes from white originally to orange. Further observation indicates that after photodeposition of Ag, the Ag/TiO_{2-x} sample gradually gets darkened as the Ag content is increased. In general, the darker the color is, the stronger the light absorption is [15,20,55]. As shown in the DRS spectra, the pure TiO_2 exhibits the lowest absorbance in the visible light region owing to its wide band gap. For TiO_{2-x}, it shows a broad absorption peak in the visible range from 400 to 650 nm wavelength in addition to the strong UV absorption below 400 nm, which can be attributed to O_V and Ti^{3+} doping [30]. All Ag/TiO_{2-x} samples show significantly enhanced absorption (with a flat plateau of > 0.45 absorbance) in the whole visible light area (400–800 nm) owing to the strong SPR absorption of Ag particles. The absorbance of Ag/TiO_{2-x} is obviously enhanced when the amount of Ag particles is increased [21,43]. In contrast, the 3%-Ag/TiO_2 also shows a similar flat plateau in the visible range but absorbance is much smaller (only ~0.15). Clearly, there is a synergy between Ti^{3+} self-doping and Ag SPR in light absorption of Ag/TiO_{2-x} in the whole visible range.

Table 1
The physical properties of the prepared photocatalysts.

Sample	S_{BET} ($m^2 \cdot g^{-1}$)	APS (nm)	PV ($cm^3 \cdot g^{-1}$)
TiO_2	17.1	14.1	0.06
TiO_{2-x}	43.8	11.8	0.13
1%-Ag/TiO_{2-x}	42.6	11.6	0.12
3%-Ag/TiO_{2-x}	56.6	15.4	0.22
5%-Ag/TiO_{2-x}	34.2	14.0	0.12
3%-Ag/TiO_2	45.7	11.9	0.14

It is known that the band gap of pristine anatase TiO_2 is about 3.2 eV, which accounts for the strong absorbance below ~400 nm wavelength. After doping with Ti^{3+} in the TiO_{2-x} sample, Ti^{3+} centers and oxygen vacancies (O_V) form donor levels underneath the CB of TiO_2 [15]. While the Ti^{3+} centers are in shallow donor states, the donor states of oxygen vacancies (O_V) is localized deeper at 0.75–1.18 eV below the CB of TiO_2 [56], which explains the broad absorption covering 400–650 nm wavelength in Fig. 5a. The Ti^{3+} centers and O_V not only serve as donor levels to increase conductivity and light absorption, but also improve the electron-hole separation in photocatalysts (as shown in later sections). Furthermore, the band gaps of TiO_2 and TiO_{2-x} can be evaluated by Kubelka-Munk function [39,40], as shown in Fig. 5b. The band gaps of bare TiO_2 and TiO_{2-x} are calculated to be 3.20 and 2.75 eV, respectively. Moreover, the inset of Fig. 5b presents the VB edges of bare TiO_2 (2.80 eV) and TiO_{2-x} (2.60 eV), respectively. Thus the CB of the TiO_{2-x} and the pristine TiO_2 is 0.40 eV and −0.15 eV vs. NHE, respectively [7,15].

3.3. Photocatalytic activity

For the study of the photocatalytic ability of the as-prepared composites, visible light photodegradation experiment was conducted for RhB aqueous solution. After incubation in the dark for 120 min before the photocatalytic degradation experiment, it can be found that less than 10% of RhB was adsorbed on the photocatalyst surface [52]. The degradation process started under visible light illumination. As shown in Fig. 6a, the pristine TiO_2 expresses the worst photocatalytic performances in degrading RhB. TiO_{2-x} and all the composites exhibit higher photocatalytic activity than the pristine TiO_2. About 26.0%, 91.4%, 95.5%, 97.6%, 94.7% and 89.9% of RhB was removed by pure TiO_2, TiO_{2-x}, 1%-Ag/TiO_{2-x}, 3%-Ag/TiO_{2-x}, 5%-Ag/TiO_{2-x} and 3%-Ag/TiO_2, respectively, after 100 min illumination. The degradation rate of 26.0% for the pure TiO_2 may be ascribed to synergistic effects of photocatalysis and dye sensitization [57,58]. Among all these samples, the highest degradation rate of 3%-Ag/TiO_{2-x} was 97.6%, which is about 3.7 times that of TiO_2 (26.0%). Apparently, this improvement in photocatalysis is primarily due to Ti^{3+} doping and further enhanced by the plasmonics from the Ag nanoparticles dispersed on the surface of the porous TiO_2 structure. These two factors synergistically accelerate electron transport, promote photogenerated charge carriers separation, and consequently enhance the catalytic performance [25,31]. The overall effect is much larger than simply adding them up.

Typically, the photocatalytic degradation reaction kinetics are expressed as $\ln (C_o/C_t) = kt$ and abides a pseudo-first order reaction [38,40]. Fig. 6b shows the comparison of the apparent rate constant k of pristine TiO_2, TiO_{2-x}, 1%-Ag/TiO_{2-x}, 3%-Ag/TiO_{2-x}, 5%-Ag/TiO_{2-x} and 3%-Ag/TiO_2 samples in visible light degradation of RhB. The 3%-Ag/TiO_{2-x} composite sample exhibited the highest photocatalytic activity ($35.6 \times 10^{-3}\ min^{-1}$), which is about 14.0 times of pristine TiO_2 ($2.53 \times 10^{-3}\ min^{-1}$). The 3%-Ag/$TiO_{2-x}$ sample balanced the demand for larger heterojunction interface and avoiding Ag particle aggregation. The high photocatalytic performance of 3%-Ag/TiO_{2-x} heterojunctions may be assigned to the broadened absorption ranging from UV to visible light and the presence of Ti^{3+} and O_V defects which improve the separation of photo-excited electrons and accelerate the electron transfer. The photothermal effect under strong SPR may also contribute to improving photocatalytic degradation ability [16].

It can be seen from the capture experiment in Fig. 6c that, 97.6% of RhB was degraded after 100 min irradiation without trapping agent in the presence of 3%-Ag/TiO_{2-x} sample. In contrast, after adding scavengers containing ($\bullet O_2^-$, p-BQ), (h^+, Na_2-EDTA) and ($\bullet$OH, TBA), the percentage of degradation of RhB decreased to 9.9%, 71.1% and 91.0%, respectively. Obviously, the photodegradation of RhB was significantly decreased in the presence of p-BQ, indicating that the superoxide radical ($\bullet O_2^-$) is the main active substance of RhB decomposition. The presence of Na_2-EDTA inhibits degradation to a certain extent, and

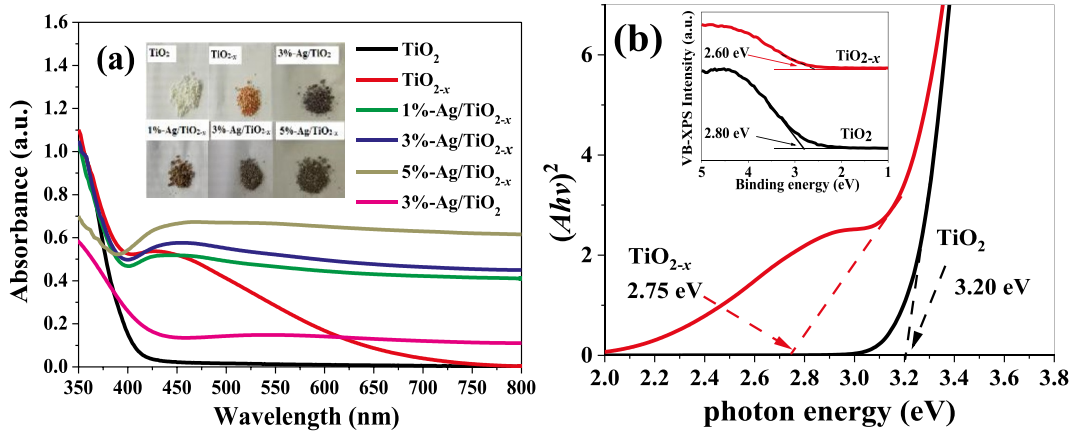

Fig. 5. (a) The UV–vis diffuse reflectance spectra and optical photos (the inset) of all catalysts, (b) the curves of the $(ahv)^2$ versus photon energy and valence band XPS spectra (the inset) of TiO_2 and TiO_{2-x} photocatalysts.

photoinduced holes (h^+) are secondary reactive species. TBA (•OH scavenger) had a relatively smaller inhibitory effect on RhB degradation. Therefore, •OH radicals play a less important role in the RhB decomposition.

In addition, the photocatalytic performance of the as-obtained powders was also evaluated in photocatalytic H_2 evolution under the irradiation of both the visible light and the full solar light. Figs. 6d and e displays the average hydrogen production rates and the kinetic curve during the 3 h photocatalytic hydrogen production process with different photocatalysts, using triethanolamine as an electron donor sacrificial agent under the visible light. In Fig. 6d, the hydrogen generation rates were 7.0, 23.2, 26.4, 37.1, 28.3 and 20.8 μmol•h^{-1}•g^{-1} for TiO_2, TiO_{2-x}, 1%-Ag/TiO_{2-x}, 3%-Ag/TiO_{2-x}, 5%-Ag/TiO_{2-x} and 3%-Ag/TiO_2, respectively. It is obvious that the pristine TiO_2 catalyst showed only a low performance for hydrogen production. But the rate with TiO_{2-x} is about 3.3 times higher. The O_V sites (oxygen vacancies) and Ti^{3+} centers in the doped TiO_2 are apparently favorable to the separation of photogenerated charges, thus vastly enhance the H_2 production [20]. After incorporating silver particles into TiO_{2-x}, the hydrogen evolution rate was boosted as the Ag loading was increased to 3%, but then dropped with further increase of Ag loading to 5%. It is known that either too much or too little Ag depositing on TiO_2 photocatalyst is unfavorable to H_2 evolution [5]. Thereinto, the 3%-Ag/TiO_{2-x} exhibited the highest H_2 generation rate, which is 5.3 times of the rate by the pristine TiO_2. In contrast, 3%-Ag/TiO_2 showed a much lower rate than 3%-Ag/TiO_{2-x}. These results demonstrate that both Ag SPR and the Ti^{3+} doping played vital roles in the enhancement of photocatalytic activity for H_2 evolution [31,53]. This is probably due to the synergistic effects of these two factors. Furthermore, upon irradiation of the full solar light, the H_2 production rates with all catalysts were more than 20 times higher, but that of 3%-Ag/TiO_{2-x} exhibits much more dramatic increase, becoming about 15.7 times of that of the pristine TiO_2 (Figs. S1a and b, Supporting Information). The comparison with other work with similar catalysts on photocatalytic H_2 production is summarized in Table S1. As seen clearly, our low-cost processes can be operated in very simple and safe condition, and exhibits the outstanding H_2 evolution (2370 μmol•h^{-1}•g^{-1}). The 3%-Ag/TiO_{2-x} hybrid shows obvious advantages over the other reported TiO_{2-x}-based composite materials [3,20,25,31,37,49]. Additionally, in order to evaluate the stability and recyclability of the 3%-Ag/TiO_{2-x} photocatalyst, the recycling experiment was carried out under the same conditions. As shown in Fig. 6f, the average H_2 evolution rate of 3%-Ag/TiO_{2-x} remains basically unchanged during the 3 cycles of photocatalytic reactions under the visible light.

3.4. Photoelectrochemical measurements

In general, the photocurrent density of a sample can also reflect its photocatalytic activity. To further evaluate the capability of as-obtained samples, a set of photoelectrochemical (PEC) tests were carried out in 0.5 M Na_2SO_4 aqueous solution. Fig. 7a shows the transient photocurrent densities when the light illumination was repeatedly turned on and off in every 60 s. A rapid photocurrent response is observed for the 3%-Ag/TiO_{2-x} sample with the highest photocurrent density. The photocurrent density of 3%-Ag/TiO_{2-x} rapidly reaches a steady-state value in about 40 s when the light is turned on. As the illumination light is turned off, the photocurrent density of 3%-Ag/TiO_{2-x} immediately returns to zero. During on/off a process of each switch, a gradual decay can be observed, which means that the photoinduced e^--h^+ pairs were experiencing a recombination process before achieving the stable state [22]. As observed in Fig. 7a, the pure TiO_2 exhibits a very weak light current response, which may be attributed to its wide band gap, resulting in very small visible light absorption of TiO_2 [18]. After the introduction of Ag, the photocurrent density slightly increases, which could be attributed to the SPR effect. Over three fold of photocurrent response is observed with TiO_{2-x}, indicating the strong light absorption and the separation of photo-induced carriers were accelerated due to the Ti^{3+} self-doping [3]. The photocurrent density was dramatically boosted by 15 times in 3%-Ag/TiO_{2-x} after incorporating Ag micro-/nano-particles, implying that a much larger amount of free electrons and holes were generated. Importantly, Ag SPR does not have much enhancement to the pristine TiO_2. There is a clear synergistic effect of the SPR of Ag and Ti^{3+} self-doping, which collectively boosted the visible-light absorption and facilitated the charge separation in 3%-Ag/TiO_{2-x} [23]. For the Ag/TiO_{2-x}.composites, when the silver content is lower or higher than 3%, the photocurrent density is decreased. Additionally, the photocurrent response exhibits good reproducibility by four light on/off cycles, which means the good chemical stability of the prepared photocatalysts [22].

The electrochemical properties of as-obtained all photocatalysts are studied by the electrochemical impedance spectra (EIS), as depicted in Fig. 7b. All EIS in the measured frequency range only show a portion of the expected semicircle feature of a typical Randle circuit, but it can be extrapolated that charge transfer resistance R_{ct} (i.e. the real impedance value of the EIS semicircle) follows the order of TiO_2 > 3%-Ag/TiO_2 > TiO_{2-x} > 1%-Ag/TiO_{2-x} > 5%-Ag/TiO_{2-x} > 3%-Ag/TiO_{2-x}. Obviously, the R_{ct} value of the TiO_{2-x} is smaller than that of the pure TiO_2, confirming the importance of Ti^{3+} doping [20]. Furthermore, the R_{ct} value of 3%-Ag/TiO_{2-x} is also smaller than that of TiO_{2-x}, illustrating the enhanced electrical conductance by Ag micro-/nano-particles and meaning to a faster photo-induced electron transition [23,25]. Especially, 3%-Ag/TiO_{2-x} photocatalyst possesses the smallest interfacial

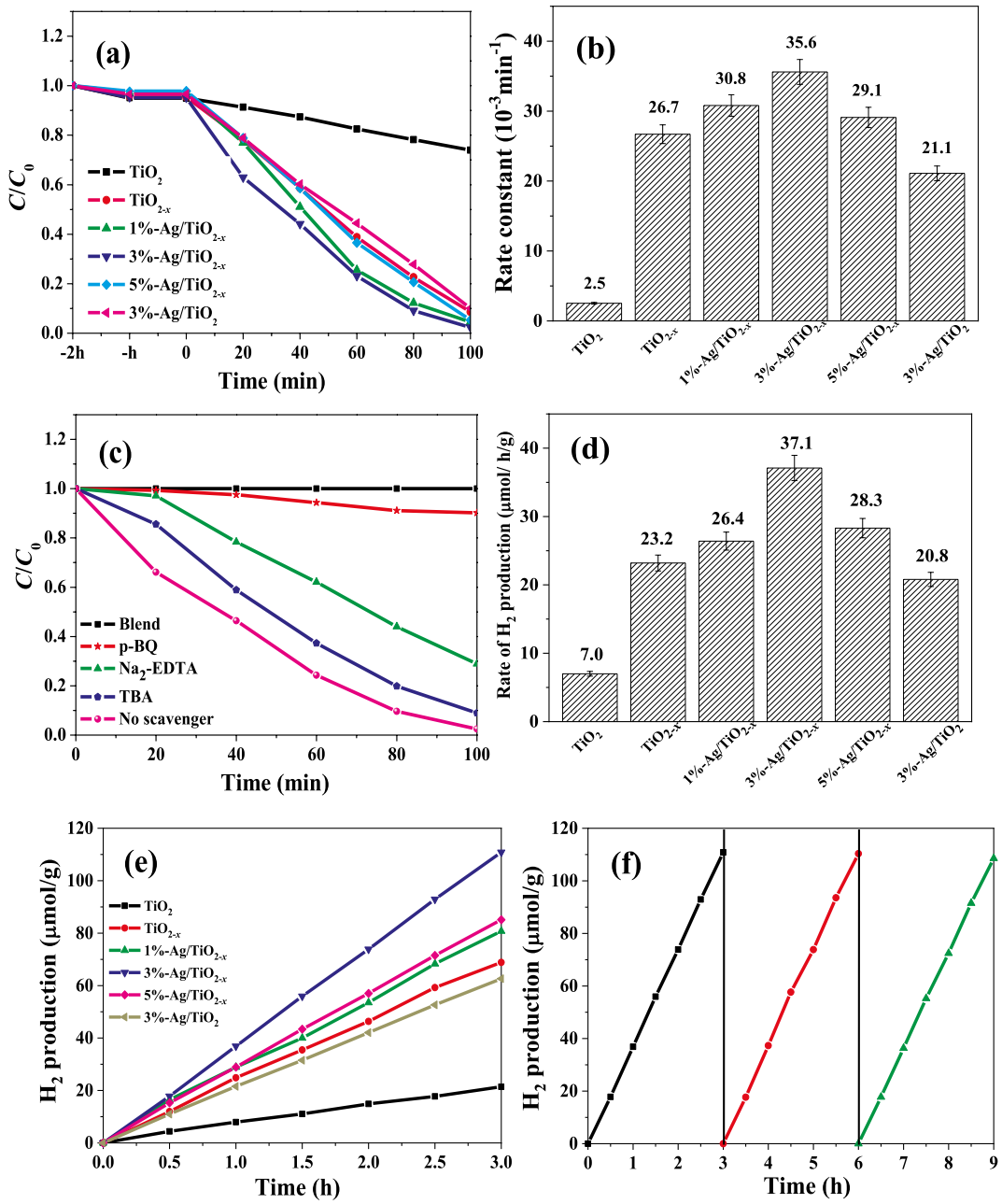

Fig. 6. (a) The kinetic curves of visible-light degradation of RhB with different catalysts, (b) comparison of the k value (10^{-3} min^{-1}) of each catalyst in visible-light degradation of RhB, (c) active species trapping experiments of the 3%-Ag/TiO_{2-x} photocatalyst under visible light irradiation, (d) the average visible-light hydrogen production rate of the prepared catalysts, (e) the kinetic visible-light hydrogen production curves of all catalysts and (f) stability test of 3%-Ag/TiO_{2-x} composite for visible-light H_2 production.

resistance, which improves the separation of photogenerated charges and reduces the recombination of e^--h^+ pairs [45,52,59]. This is consistent with its highest photoelectrochemical performance. The synergistic effect of Ti^{3+} self-doping and Ag SPR may be the main factor for the low R_{ct} value.

3.5. Mechanism of photocatalytic activity enhancement

From the above results, it is apparent that the Ag/TiO_{2-x} hybrid materials have significantly enhanced photocatalytic activity in RhB photodegradation and photocatalytic hydrogen production. In general, Ag NPs may serve as a co-catalyst in the photocatalytic degradation of RhB [43,60,61]. However, the photocatalytic efficiency of silver as a cocatalyst is not high [60]. In our work, plasmonic effect of Ag NPs can be clearly observed by a characteristic SPR peak *ca.* 450 nm in UV–vis absorbance spectra (see Fig. 5a). This further confirms that Ag NPs plasmonic effect plays an important role in photoreaction of RhB. Therefore, the significantly enhanced photocatalytic activity can be consistently explained by the synergistic effects of Ag SPR and Ti^{3+} doping in the shallow TiO_2 surface layer. Fig. 8a illustrates the energy diagram and light absorption properties of the Ag micro-/nano-particles and Ti^{3+}-doped TiO_2 before they are put in contact. As we discussed earlier in the DRS, Ti^{3+} doping to TiO_2 (in the sample denoted as TiO_{2-x}) creates shallow Ti^{3+} centers and O_V sites as donor levels spanning from the bottom of the CB to about 0.25–1.18 eV below (see Fig. 8b), which induces the strong absorption in the visible range from ~400 nm to ~650 nm in the UV–vis absorption spectra in Fig. 5a. This dramatically increases the capability to generate separated e^--h^+ pairs by

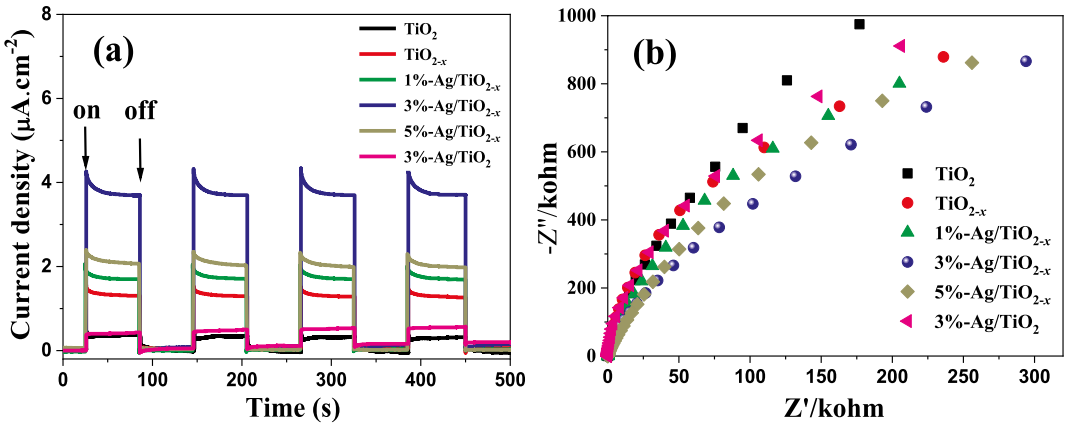

Fig. 7. (a) Photocurrent response and (b) EIS Nyquist plots of all catalysts under visible light.

visible light, but the electrons are most trapped at the defect sites (Ti^{3+} and O_V) near the surface of TiO_{2-x}. On the other hand, the Ag micro-/nano-particles produce strong SPR [43], leading to enhanced light absorption with a nearly constant absorbance (~0.15) in the whole visible range of ~400 nm–~800 nm. However, the SPR only causes collective electron oscillation in the Ag particles and the absorbed photon energy is low in the long visible wavelength range. Thus the SPR alone is insufficient to cause photochemical reactions. Overall, the SPR of isolated Ag particles and Ti^{3+}-doping each alone only enhance the photocatalytic activity to a limited degree.

When the Ag micro-/nano-particles are deposited on both pristine TiO_2 and the Ti^{3+}-doped TiO_2 (i.e., TiO_{2-x}) to form hybrid materials, it creates an interesting metal-semiconductor heterojunction as shown in Fig. 8b. This leads to a Schottky barrier represented by a sharp potential increase by φ_B at the junction and a diffusive potential drop φ_{bi} in the depletion layer extending from the interface to bulk TiO_{2-x}. The Schottky barrier height φ_B is determined as $\varphi_B = \varphi_{Ag} - \chi_{TiO2} = \sim 0.39$ eV [62], where $e\varphi_{Ag}$ equals to the work function of Ag metal and χ_{TiO2} is the electron affinity of the pristine TiO_2. The built-in barrier height φ_{bi} varies with the applied voltage bias. Without light illumination, some electrons are readily transferred from TiO_2 to Ag metal through this heterojunction barrier and get trapped in the Ag micro-/nano-particles. This is one of the reasons that the Ag 3d peaks in Ag/TiO_{2-x} hybrids shift to lower binding energy by ~1.3 eV in XPS (Fig. 2d). Interestingly, the absorbance of Ag/TiO_{2-x} (see Fig. 5a), particularly at wavelength over ~600 nm, is significantly higher than the simple sum of the absorbance of Ag (dominated by SPR) and TiO_{2-x} (dominated by excitation from VB to Ti^{3+}/O_V states). This phenomenon and the improved photocatalytic activity of Ag/TiO_{2-x} strongly indicate a synergistic coupling between Ag SPR and Ti^{3+}-doping [31].

The schematic energy diagram in Fig. 8b illustrates the possible mechanism for the synergistic enhancement in Ag/TiO_{2-x} under visible light illumination. There are two key factors. First, the SPR provides strong absorption of visible light. Even though SPR does not generate electron-hole separation alone, it provides sufficient energy to generate "hot electrons" that can surmount the Schottky barrier and are injected into the CB of TiO_{2-x}. These hot electrons become active free electrons and can now induce photochemical reactions. Second, the energy due to photon absorption by SPR in the visible wavelength can be transferred to the Ti^{3+}/O_V states in TiO_{2-x} through the mechanism called plasmon-induced resonance energy transfer (PIRET) [6,63–65]. This provides sufficient energy to excite the trapped electrons in the Ti^{3+}/O_V states that are generated by TiO_{2-x} absorption between 400 and 650 nm. These two effects are particularly effective in enhancing the utilization of visible light at longer wavelength range (> ~600 nm). In addition, both of these two processes lead to improved e^--h^+ separation by transferring electrons to the CB of TiO_2 and migrating holes to Ag micro-/nano-particles. As a result, the Schottky barrier at the heterojunction of Ag/TiO_{2-x} photocatalysts could explain the synergistic enhancement owing to the strong coupling between Ti^{3+}-doping and the Ag SPR [7,23,25].

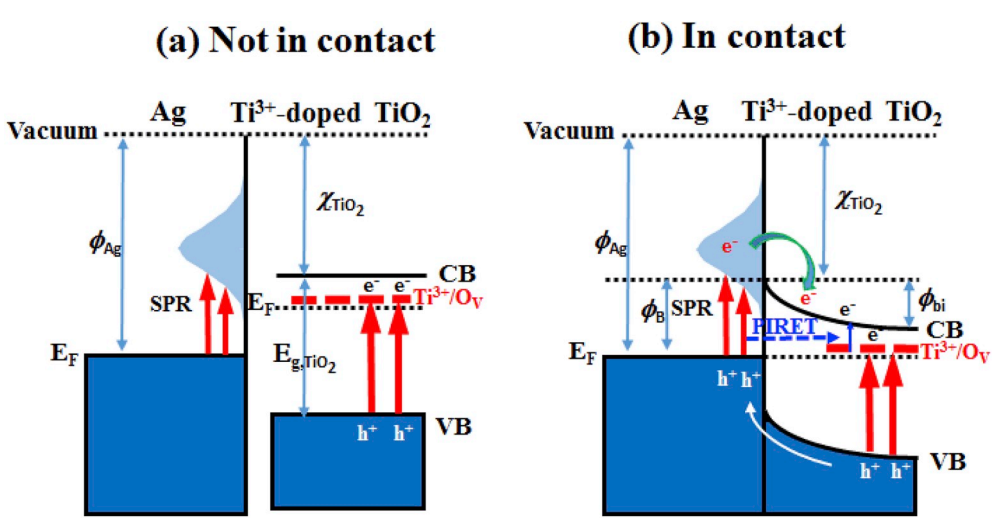

Fig. 8. Schematic energy diagram of the Ag micro-/nano-particles and TiO_{2-x} (Ti^{3+}-doped TiO_2) framework (a) before and (b) after forming the heterojunction.

4. Conclusions

In summary, we have successfully fabricated Ag/TiO_{2-x} heterojunction-based photocatalysts through a simple microwave-assisted reaction with vitamin C as a reductant to dope the macro-/meso-porous anatase TiO_2 framework with Ti^{3+} followed by photo-deposition of Ag macro-/nano-particles. These low-cost processes can be applied in gentle and safe conditions for the rapid synthesis of Ti^{3+}-doped TiO_2. In photodegradation of RhB and photocatalytic production of H_2 using visible light, the Ag/TiO_{2-x} photocatalysts present significantly enhanced photocatalytic activity than the control systems with only Ti^{3+} doping (as in TiO_{2-x}) or Ag SPR (as in Ag/TiO_2). The materials characterization and photochemical studies consistently reveal the synergistic improvement of the photocatalytic properties due to the coupling between the SPR of the Ag macro-/nano-particles and Ti^{3+} or oxygen vacancy states in TiO_{2-x}, which can be explained by the formation of a Schottky barrier at the Ag/TiO_{2-x} junction.

Declaration of competing interest

The authors declare that they have no known competing financial interests or personal relationships that could have appeared to influence the work reported in this paper.

Acknowledgements

JL acknowledges the partial support in materials characterization/processing and personnel by NSF grants (CBET-1703263 and DMR-1707585).

Appendix A. Supplementary data

Supplementary data to this article can be found online at https://doi.org/10.1016/j.ceramint.2020.01.073.

References

[1] S.H. Shen, J. Chen, M. Wang, X. Sheng, X.Y. Chen, X.J. Feng, S.S. Mao, Titanium dioxide nanostructures for photoelectrochemical applications, Prog. Mater. Sci. 98 (2018) 299–385.
[2] B.S. Liu, X.J. Zhao, J.G. Yu, I.P. Parkin, A. Fujishima, K. Nakata, Intrinsic intermediate gap states of TiO_2 materials and their roles in charge carrier kinetics, J. Photochem. Photobiol. C 39 (2019) 1–57.
[3] C. Liu, P.C. Wu, J.N. Wu, J. Hou, H.C. Bai, Z.Y. Liu, Effective protect of oxygen vacancies in carbon layer coated black TiO_{2-x}/CNNS hetero-junction photocatalyst, Chem. Eng. J. 359 (2019) 58–68.
[4] C. He, J. Cheng, X. Zhang, M. Douthwaite, S. Pattisson, Z.P. Hao, Recent advances in the catalytic oxidation of volatile organic compounds: a review based on pollutant sorts and sources, Chem. Rev. 119 (2019) 4471–4568.
[5] Z. Wang, Q. Yang, W.L. Liu, H. Ran, C.L. Zhang, X.Y. Han, X.Y. He, X. Wang, C.G. Hu, Optical porous hollow-boxes assembled by $SrSO_4$/TiO_2/Pt nanoparticles for high performance of photocatalytic H_2 evolution, Nano Energy 59 (2019) 129–137.
[6] V. Kumaravel, S. Mathew, J. Bartlett, S.C. Pillai, Photocatalytic hydrogen production using metal doped TiO_2: a review of recent advances, Appl. Catal. B Environ. 244 (2019) 1021–1064.
[7] K.K. Paul, P.K. Giri, Role of surface plasmons and hot electrons on the multi-step photocatalytic decay by defect enriched Ag@TiO_2 nanorods under visible light, J. Phys. Chem. C 121 (2017) 20016–20030.
[8] Y.O. Wang, H.J. Suzuki, J.J. Xie, O. Tomita, D.J. Martin, M. Higashi, D. Kong, R. Abe, J.W. Tang, Mimicking natural photosynthesis: solar to renewable H_2 fuel synthesis by Z-scheme water splitting systems, Chem. Rev. 118 (2018) 5201–5241.
[9] H.G. Yu, H.T. Li, P. Wang, X.Q. Yi, Edge-selectivelyamidatedgraphene for boosting H_2-evolution activity of TiO_2 photocatalyst, Appl. Catal. B Environ. 264 (2020) 118504.
[10] N.C. Zheng, T. Ouyang, Y.B. Chen, Z. Wang, D.Y. Chen, Z.Q. Liu, Ultrathin CdS shell-sensitized hollow S-doped CeO2 spheres for efficient visible-light photocatalysis, Catal. Sci. Technol. 9 (2019) 1357–1364.
[11] X.H. Wu, X.F. Wang, F.Z. Wang, H.G. Yu, Soluble g-C_3N_4 nanosheets: facile synthesis and application in photocatalytic hydrogen evolution, Appl. Catal. B Environ. 247 (2019) 70–77.
[12] G. Yang, D.M. Chen, H. Ding, J.J. Feng, J.Z. Zhang, Y.F. Zhu, S. Hamid, D.W. Bahnemann, Well-designed 3D $ZnIn_2S_4$ nanosheets/TiO_2 nanobelts as direct Z-scheme photocatalysts for CO_2 photoreduction into renewable hydrocarbon fuel with high efficiency, Appl. Catal. B Environ. 219 (2017) 611–618.
[13] H.G. Yu, Y. Huang, D.D. Gao, P. Wang, H. Tang, Improved H_2-generation performance of Pt/CdS photocatalyst by a dual-function TiO_2 mediator for effective electron transfer and hole blocking, Ceram. Int. 45 (2019) 9807–9813.
[14] K. Wang, X.Y. Wu, G.K. Zhang, J. Li, Y. Li, $Ba_5Ta_4O_{15}$ nanosheet/$AgVO_3$ nanoribbon heterojunctions with enhanced photocatalytic oxidation performance: hole dominated charge transfer path and plasmonic effect insight, ACS Sustain. Chem. Eng. 6 (2018) 6682–6692.
[15] L. Xu, X. Bai, L.K. Guo, S.J. Yang, P.K. Jin, L. Yang, Facial fabrication of carbon quantum dots (CDs)-modified N-TiO_{2-x} nanocomposite for the efficient photoreduction of Cr (VI) under visible light, Chem. Eng. J. 357 (2019) 473–486.
[16] T.Y. Zhao, Z.P. Xing, Z.Y. Xiu, Z.Z. Li, P. Chen, Q. Zhu, W. Zhou, Synergistic effect of surface plasmon resonance, Ti^{3+} and oxygen vacancy defects on Ag/MoS_2/TiO_{2-x} ternary heterojunctions with enhancing photothermal catalysis for low-temperature wastewater degradation, J. Hazard Mater. 364 (2019) 117–124.
[17] H.Z. Li, L.Y. Shen, K.F. Zhang, B.J. Sun, L.P. Ren, P.Z. Qiao, K. Pan, L. Wang, W. Zhou, Surface plasmon resonance-enhanced solar-driven photocatalytic performance from Ag nanoparticle-decorated self-floating porous black TiO_2 foams, Appl. Catal. B Environ. 220 (2018) 111–117.
[18] G. Liu, G.H. Wang, Z.H. Hu, Y.R. Su, L. Zhao, Ag_2O nanoparticles decorated TiO_2 nanofibers as a p-n heterojunction for enhanced photocatalytic decomposition of RhB under visible light irradiation, Appl. Surf. Sci. 465 (2019) 902–910.
[19] X.F. Wu, Y. Sun, H. Li, Y.J. Wang, C.X. Zhang, J.R. Zhang, J.Z. Su, Y.W. Wang, Y. Zhang, C. Wang, M. Zhang, In-situ synthesis of novel p-n heterojunction of Ag_2CrO_4-$Bi_2Sn_2O_7$ hybrids for visible-light-driven photocatalysis, J Alloy. Compd. 740 (2018) 1197–1203.
[20] Y. Cao, Z.P. Xing, Y.C. Shen, Z.Z. Li, X.Y. Wu, X. Yan, J.L. Zou, S.L. Yang, W. Zhou, Mesoporous black Ti^{3+}/N-TiO_2 spheres for efficient visible-light-driven photocatalytic performance, Chem. Eng. J. 325 (2017) 199–207.
[21] Y.X. Dong, X.L. Wang, E.M. Jin, S.M. Jeong, B. Jin, S.H. Lee, One-step hydrothermal synthesis of Ag decorated TiO_2 nanoparticles for dye-sensitized solar cell application, Renew. Energy 135 (2019) 1207–1212.
[22] Q.L. Zeng, X.F. Xie, X. Wang, Y. Wang, G.H. Lu, D.Y.H. Pui, J. Sun, Enhanced photocatalytic performance of Ag@TiO_2 for the gaseous acetaldehyde photodegradation under fluorescent lamp, Chem. Eng. J. 341 (2018) 83–92.
[23] Y.Y. Duan, M. Zhang, L. Wang, F. Wang, L.P. Yang, X.Y. Li, C.Y. Wang, Plasmonic Ag-TiO_{2-x} nanocomposites for the photocatalytic removal of NO under visible light with high selectivity: the role of oxygen vacancies, Appl. Catal. B Environ. 204 (2017) 67–77.
[24] T. Cai, Y.T. Liu, L.L. Wang, S.Q. Zhang, J.H. Ma, W.Y. Dong, Y.X. Zeng, J.L. Yuan, C.B. Liu, S.L. Luo, "Dark deposition" of Ag nanoparticles on TiO_2: improvement of electron storage capacity to boost "memory catalysis" activity, ACS Appl. Mater. Interfaces 10 (2018) 25350–25359.
[25] J.J. Jiang, Z.P. Xing, M. Li, Z.Z. Li, J.W. Yin, J.Y. Kuang, J.L. Zou, Q. Zhu, W. Zhou, Plasmon Ag decorated 3D urchinlike N-TiO_{2-x} for enhanced visible-light-driven photocatalytic performance, J. Colloid Interface Sci. 521 (2018) 102–110.
[26] D.M. Chen, Z.H. Wang, T.Z. Ren, H. Ding, W.Q. Yao, R.L. Zong, Y.F. Zhu, Influence of defects on the photocatalytic activity of ZnO, J. Phys. Chem. C 118 (2014) 15300–15307.
[27] D.X. Tan, J.L. Zhang, J.B. Shi, S.P. Li, B.X. Zhang, X.N. Tan, F.Y. Zhang, L.F. Liu, D. Shao, B.X. Han, Photocatalytic CO_2 transformation to CH_4 by Ag/Pd bimetals supported on N-doped TiO_2 nanosheet, ACS Appl. Mater. Interfaces 10 (2018) 24516–24522.
[28] D.L. Qian, D.Y. Chen, N.J. Li, Q.F. Xu, H. Li, J.H. He, J.M. Lu, TiO_2/sulfonated graphene oxide/Ag nanoparticle membrane: in situ separation and photodegradation of oil/water emulsions, J. Membr. Sci. 554 (2018) 16–25.
[29] X.B. Chen, L. Liu, P.Y. Yu, S.S. Mao, Increasing solar absorption for photocatalysis with black hydrogenated titanium dioxide nanocrystals, Science 331 (2011) 746–750.
[30] G. Zhou, H.Y. Meng, Y. Cao, X.J. Kou, S.X. Duan, L.L. Fan, M. Xiao, F.Z. Zhou, Z.Z. Li, Z.P. Xing, Surface plasmon resonance-enhanced solar-driven photocatalytic performance from Ag nanoparticles-decorated Ti^{3+} self-doped porous black TiO_2 pillars, J. Ind. Eng. Chem. 64 (2018) 188–193.
[31] M. Li, Z.P. Xing, J.J. Jiang, Z.Z. Li, J.W. Yin, J.Y. Kuang, S.Y. Tan, Q. Zhu, W. Zhou, Surface plasmon resonance-enhanced visible-light-driven photocatalysis by Ag nanoparticles decorated S-TiO_{2-x} nanorods, J. Taiwan. Inst. Chem. Eng. 82 (2018) 198–204.
[32] Y.W. Wang, C.W. Chen, J.H. Hsieh, W.J. Tseng, Preparation of Ag/TiO_2 composite foams via pickering emulsion for bactericide and photocatalysis, Ceram. Int. 43 (2017) S797–S801.
[33] H.G. Yu, W.J. Liu, X.F. Wang, F.Z. Wang, Promoting the interfacial H_2-evolution reaction of metallic Ag by Ag_2S cocatalyst: a case study of TiO_2/Ag-Ag_2S photocatalyst, Appl. Catal. B Environ. 225 (2018) 415–423.
[34] H.L. Ran, J.J. Fan, X.L. Zhang, J. Mao, G.S. Shao, Enhanced performances of dye-sensitized solar cells based on Au-TiO_2 and Ag-TiO_2 plasmonic hybrid nanocomposites, Appl. Surf. Sci. 430 (2018) 415–423.
[35] X. He, Y. Guo, J.H. Liu, X. Li, J.Y. Qi, Fabrication of peanut-like TiO_2 microarchitecture with enhanced surface light trapping and high specific surface area for high-efficiency dye sensitized solar cells, J. Power Sources 423 (2019) 236–245.
[36] J. Wang, G.H. Wang, X.H. Wei, G. Liu, J. Li, ZnO nanoparticles implanted in TiO_2 macrochannels as an effective direct Z-scheme heterojunction photocatalyst for degradation of RhB, Appl. Surf. Sci. 456 (2018) 666–675.
[37] J.Q. Pan, Z.J. Dong, B.B. Wang, Z.Y. Jiang, C. Zhao, J.J. Wang, C.S. Song, Y.Y. Zheng, C.R. Li, The enhancement of photocatalytic hydrogen production via Ti^{3+} self-doping black TiO_2/g-C_3N_4 hollow core-shell nano-heterojunction, Appl. Catal. B Environ. 242 (2019) 92–99.

[38] L.Y. Lu, G.H. Wang, M. Zou, J. Wang, J. Li, Effects of calcining temperature on formation of hierarchical TiO_2/g-C_3N_4 hybrids as an effective Z-scheme heterojunction photocatalyst, Appl. Surf. Sci. 441 (2018) 1012–1023.
[39] J. Wang, G.H. Wang, X. Wang, Y. Wu, Y.R. Su, H. Tang, 3D/2D direct Z-scheme heterojunctions of hierarchical TiO_2 microflowers/g-C_3N_4 nanosheets with enhanced charge carrier separation for photocatalytic H_2 evolution, Carbon 149 (2019) 618–626.
[40] R.R. Hao, G.H. Wang, H. Tang, L.L. Sun, C. Xu, D.Y. Han, Template-free preparation of macro/mesoporous g-C_3N_4/TiO_2 heterojunction photocatalysts with enhanced visible light photocatalytic activity, Appl. Catal. B Environ. 187 (2016) 47–58.
[41] Y. Ma, N. Wang, J. Chen, C.S. Chen, H.S. San, J.G. Chen, Z.D. Cheng, Betavoltaic enhancement using defect-engineered TiO_2 nanotube arrays through electrochemical reduction in organic electrolytes, ACS Appl. Mater. Interfaces 10 (2018) 22174–22181.
[42] Z.L. Huang, G.W. Meng, X.Y. Hu, Q.J. Pan, D.X. Huo, H.J. Zhou, Y. Ke, N. Wu, Plasmon-tunable Au@Ag core-shell spiky nanoparticles for surface-enhanced Raman scattering, Nano Res. 12 (2019) 449–455.
[43] I. Majeed, U. Manzoor, F.K. Kanodarwala, M.A. Nadeem, E. Hussain, H. Ali, A. Badshah, J.A. Stride, M.A. Nadeem, Pd-Ag decorated g-C_3N_4 as an efficient photocatalyst for hydrogen production from water under direct solar light irradiation, Catal. Sci. Technol. 8 (2018) 1183–1193.
[44] Y. Zhang, T. Wang, M. Zhou, Y. Wang, Z.M. Zhang, Hydrothermal preparation of Ag-TiO_2 nanostructures with exposed {001}/{101} facets for enhancing visible light photocatalytic activity, Ceram. Int. 43 (2017) 3118–3126.
[45] X.G. Wang, M.H. Sun, M. Murugananthan, Y.R. Zhang, L.Z. Zhang, Electrochemically self-doped WO_3/TiO_2 nanotubes for photocatalytic degradation of volatile organic compounds, Appl. Catal. B Environ. 260 (2020) 118205.
[46] Y. Xu, R. Ahmed, D. Klein, S. Cap, K. Freedy, S. McDonnell, G. Zangari, Improving photo-oxidation activity of water by introducing Ti^{3+} in self-ordered TiO_2 nanotube arrays treated with Ar/NH_3, J. Power Sources 414 (2019) 242–249.
[47] S. Liu, M.Y. Zhao, Z.T. He, Y. Zhong, H. Ding, D.M. Chen, Preparation of a p-n heterojunction 2D BiOI nanosheet/1D $BiPO_4$ nanorod composite electrode for enhanced visible light photoelectrocatalysis, Chin. J. Catal. 40 (2019) 446–457.
[48] G.X. Liu, W. Li, R. Bi, C.A. Etogo, X.Y. Yu, L. Zhang, Cation-assisted formation of porous TiO_{2-x} nanoboxes with high grain boundary density as efficient electrocatalysts for lithium-oxygen batteries, ACS Catal. 8 (2018) 1720–1727.
[49] J.J. Jiang, Z.P. Xing, M. Li, Z.Z. Li, X.Y. Wu, M.Q. Hu, J.F. Wan, N. Wang, A.S. Besov, W. Zhou, In situ Ti^{3+}/N-codoped three-dimensional (3D) urchinlike black TiO_2 architectures as efficient visible-light-driven photocatalysts, Ind. Eng. Chem. Res. 56 (2017) 7948–7956.
[50] M. Xu, S. He, H. Chen, G.Q. Cui, L.R. Zheng, B. Wang, M. Wei, TiO_{2-x} -modified Ni nanocatalyst with tunable metal-support interaction for water-gas shift reaction, ACS Catal. 7 (2017) 7600–7609.
[51] G.H. Yin, X.Y. Huang, T.Y. Chen, W. Zhao, Q.Y. Bi, J. Xu, Y.F. Han, F.Q. Huang, Hydrogenated blue titania for efficient solar to chemical conversions: preparation, characterization, and reaction mechanism of CO_2 reduction, ACS Catal. 8 (2018) 1009–1017.
[52] Y. Cao, Z.P. Xing, Z.Z. Li, X.Y. Wu, M.Q. Hu, X. Yan, Q. Zhu, S.L. Yang, W. Zhou, Mesoporous black TiO_{2-x}/Ag nanospheres coupled with g-C_3N_4 nanosheets as 3D/2D ternary heterojunctions visible light photocatalysts, J. Hazard Mater. 343 (2018) 181–190.
[53] N.R. Khalid, E. Ahmed, M. Ahmad, N.A. Niaz, M. Ramzan, M. Shakil, T. Iqbal, A. Majid, Microwave-assisted synthesis of Ag-TiO_2/graphene composite for hydrogen production under visible light irradiation, Ceram. Int. 42 (2016) 18257–18263.
[54] T.K. Rahul, M. Mohan, N. Sandhyarani, Enhanced solar hydrogen evolution over in situ gold-platinum bimetallic nanoparticle-loaded Ti^{3+} self-doped titania photocatalysts, ACS Sustain. Chem. Eng. 6 (2018) 3049–3059.
[55] H.G. Yu, R.R. Yuan, D.D. Gao, Y. Xu, Y.J. Xu, Ethyl acetate-induced formation of amorphous MoS_x nanoclusters for improved H_2-evolution activity of TiO_2 photocatalyst, Chem. Eng. J. 375 (2019) 121934.
[56] X.Y. Pan, M.Q. Yang, X.Z. Fu, N. Zhang, Y.J. Xu, Defective TiO_2 with oxygen vacancies: synthesis, properties and photocatalytic applications, Nanoscale 5 (2013) 3601–3614.
[57] X.X. Li, T. Wan, J.Y. Qiu, H. Wei, F.H. Qin, Y.H. Wang, Y.J. Liao, Z.Y. Huang, X.C. Tan, In-situ photocalorimetry-fluorescence spectroscopy studies of RhB photocatalysis over Z-schemeg-C_3N_4@Ag@Ag_3PO_4 nanocomposites: a pseudo-zero-order rather than a first-order process, Appl. Catal. B Environ. 217 (2017) 591–602.
[58] Y.C. Hsiao, T.F. Wu, Y.S. Wang, C.C. Hu, C. Huang, Evaluating the sensitizing effect on the photocatalytic decoloration of dyes using anatase-TiO_2, Appl. Catal. B Environ. 148–149 (2014) 250–257.
[59] X.Y. Liu, M. Ye, S.P. Zhang, G.C. Huang, C.H. Li, J.G. Yu, P.K. Wong, S.W. Liu, Enhanced photocatalytic CO_2 valorization over TiO_2 hollow microspheres by synergetic surface tailoring and Au decoration, J. Mater. Chem. A 6 (2018) 24245–24255.
[60] M. Imizcoz, A.V. Puga, Assessment of photocatalytic hydrogen production from biomass or wastewaters depending on the metal co-catalyst and its deposition method on TiO_2, Catalysts 9 (2019) 584–599.
[61] L.C. Liu, A. Corma, Metal catalysts for heterogeneous catalysis: from single atoms to nanoclusters and nanoparticles, Chem. Rev. 118 (2018) 4981–5079.
[62] Y. Wang, L. Liu, L. Xu, C. Meng, W. Zhu, Ag/TiO_2 nanofiber heterostructures: highly enhanced photocatalysts under visible light, J. Appl. Phys. 113 (2013) 174311.
[63] Y.Q. Yang, J. Wu, J. Li, Correlation of the plasmon-enhanced photoconductance and photovoltaic properties of core-shell Au@TiO_2 network, Appl. Phys. Lett. 109 (2016) 091604.
[64] S.K. Cushing, N.Q. Wu, Progress and perspectives of plasmon-enhanced solar energy conversion, J. Phys. Chem. Lett. 7 (2016) 666–675.
[65] Y.Q. Yang, H.B. Gobeze, F. D'Souza, R. Jankowiak, J. Li, Plasmonic enhancement of biosolar cells employing light harvesting complex II incorporated with core-shell metal@TiO_2 nanoparticles, Adv. Mater. Interfaces 3 (2016) 1600371.